

Manufacturing Letters

Manufacturing Letters 00 (2023) 000-000



52nd SME North American Manufacturing Research Conference (NAMRC 52, 2024)

Kinematic analysis of engagement and bending capabilities of a point-of-care, incremental skeletal fixation plate bending system

David J. Hoelzle^{a,*}, Brian Thurston^b, Javier Vazquez-Armendariz^{b,c}, Tyler Babinec^a, Luis H. Olivas-Alanis^{b,c}, Stephen Niezgoda^b, Glenn Daehn^b, David Dean^{b,d}, Robert X. Gao^e

^aDept. of Mechanical and Aerospace Engineering, Ohio State University, 201 W. 19th Ave., Columbus, OH 43210, USA ^bDept. of Materials Science and Engineering, Ohio State University, 140 W. 19th Ave., Columbus, OH 43210, USA ^cTecnologico de Monterrey, School of Engineering and Sciences, 2501 Eugenio Garza Sada Ave., 64849 Monterrey, NL, Mexico ^dDept. of Plastic and Reconstructive Surgery, Ohio State University, 915 Olentangy River Road, Columbus, OH 43212 ^eDept. of Mechanical and Aerospace Engineering, Case Western Reserve University, 2123 Martin Luther King Jr. Dr., Cleveland, OH 44106, USA

Abstract

The current standard of care for skeletal reconstruction surgery is to join skeletal disunions with fixation plates and these plates are most commonly fit to bones through manual bending. The bending procedure is often performed in the surgical operating theatre with specialized pliers or, if available, lengthy pre-operative bending to fit a 3D printed skeletal model prepared on computer as part of a virtual surgical plan. Manual bending of fixation plates by eye or to a model can take considerable time. Repetitive bending at a single location can result in work hardening that increases the subsequent risk of fatigue failure. However, incremental forming systems may provide a solution to automatically bend fixation plates accurately, rapidly, and as little at any one location as possible. This paper is an investigation of the kinematics and manipulability of two versions of an incremental fixture plate bending system for Point of Care Manufacturing (POCM) of craniomaxillofacial (CMF) skeletal fixation hardware. The Automatic Plate Bender (APB) v1 is a minimal POCM system that is designed for simple straight plates with a constant incremental pitch. The APB v2 is a more complex POCM that is designed to accommodate a larger variety of standard plates. Kinematic and manipulability analysis demonstrate the engagement and bend classes that each system can accomplish, and identifies a critical singularity in the APB v2 mechanism. The paper concludes with two case studies in which a path planning algorithm uses a manipulability analysis to avoid singularities during incremental bending.

© 2023 The Authors. Published by Elsevier Ltd. This is an open access article under the CC BY-NC-ND license (http://creativecommons.org/licenses/by-nc-nd/4.0/)

Peer-review under responsibility of the scientific committee of the NAMRI/SME.

Keywords: forming; incrmental forming; hybrid autonomous manufacturing; machine kinematics; point of care manufacturing

1. Introduction

Skeletal defects in the craniomaxillofacial (CMF) region, caused by either trauma or purposeful resection for disease treatment, such as bone resection for late stage cancer, may involve highly curving regions of the CMF skeleton that will, subsequently, undergo the cyclic loading during mastication. The current standard-of-care method to hold bone fracture or saw

lines or bone grafts during healing is metallic fixation, which is typically composed of surgical grade 5, Ti-6Al-4V alloy. These are usually flat plates with a series of predrilled holes for surgeon selected fixation to the CMF skeleton with surgical screws (Fig. 1a). Simpler cases of non-load-bearing areas of the CMF will require 1 - 3 thin plates to span and fixate fracture lines or bone grafts. Often the requirements of occlusion meant that the reconstructed skeletal geometry can have less that 250 um error [2]. Complex cases resulting from significant trauma affecting large areas of the CMF skeleton may require placement of up to 30 plates in a single, perhaps lengthy, surgery. The current clinical practice is for the surgeon to manually bend plates to fit the patient anatomy using specialty plate bending pliers. In 2213-8463 © 2023 The Authors. Published by Elsevier Ltd. This is an open access article under the CC BY-NC-ND license

^{*} Corresponding author. Tel.: +1-614-256-7388; email: hoelzle.1@osu.edu. E-mail address: hoelzle.1@osu.edu (Robert X. Gao).

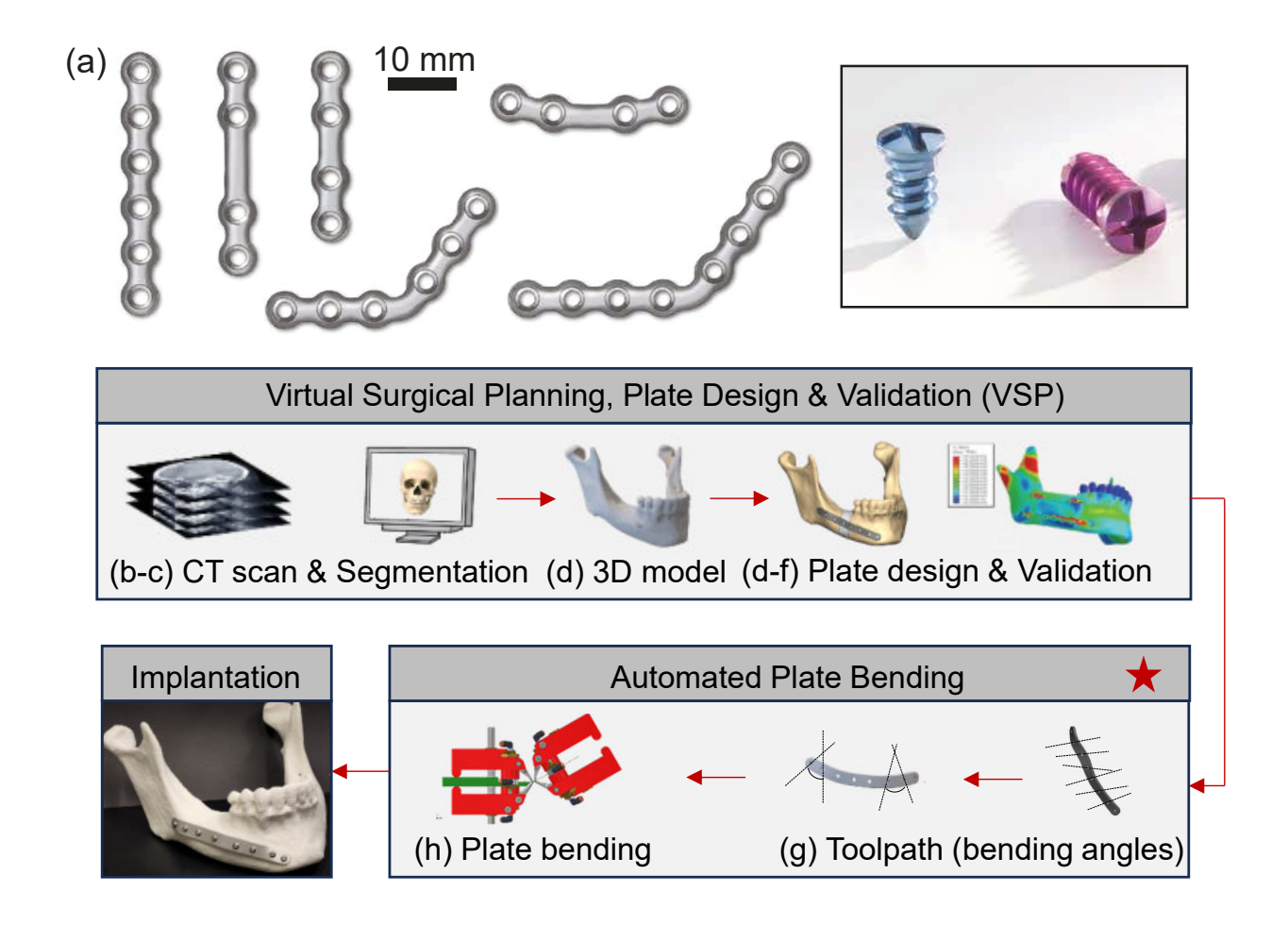


Figure 1. Fixation plate workpieces and desired workflow for a POCM system to bend skeletal fixation plates for CMF reconstruction. (a) Representative plate geometries in the as-received state, demonstrating both the straight, contant-pitch geometry and curved, variable-pitch geometries, and the screws used to fix to the patient CMF. Figures copied from KLS Martin literature (https://www.klsmartin.com/en-na/). (b-c) Computed tomography (CT) scan and automated segmentation to create a 3D surface representation of the patient CMF anatomy, and then 3D model volume representation (d) for VSP plate design (e) and finite element model (f) validation [5]. Either in the surgical theatre or in the same medical facility, incremental forming system, such as those described as Automatic Plate Bender v1 or v2 would take the bending angles α , β , and γ from the plate design (g) and automatically bend and validate plate accuracy and work hardening accumulation (h). The finished plate would then be fixed to the patient. Figure modified from [8] with Permission.

cases that permit extended preoperative planning, the plates are bent prior to the surgery against a 3D printed reference model generated during a virtual (i.e., 3D CT computer-based) surgical planning session. In emergency trauma cases, the plates are iteratively bent and placed on the patient to compare profile accuracy, significantly increasing surgical time. In both cases the plates experience work hardening, which is heuristically known to lead to plate failure and thus revision surgeries.

In both the preoperative and emergency scenarios, this lengthy, *ad hoc*, and surgeon experience and judgement-dependent plate bending process could be significantly aided with a re-envisioned work- flow (Fig. 1) [8]: 1) Given a normative model to compare with the patient's CMF anatomy, a virtual surgical planning (VSP) software could assist the surgeon in the choice of stock fixation plate hardware dimensions, placement of the plate(s) and screw locations; 2) from plate placement, a geometric model of the plate conformally fixated to the CMF structure would provide screw hole normal vec-

tors, which can then be expressed as a sequence of hole-to-hole incremental bends with three degrees of rotational freedom, denoted as α_k , β_k , and γ_k for the k^{th} hole, representing the yaw, pitch, roll of each hole-to-hole increment; 3) at the point of care, an incremental plate forming system would incrementally form each plate, whilst validating that each plate meets geometric accuracy specifications while not exceeding engineering metrics of work hardening limits.

Critical to realizing this vision of POCM for CMF fixation hardware is developments in virtual surgical planning [8], incremental fixture plate forming machine design [9], and process validation. This paper investigates two different incremental fixture plate forming POCM systems: The automatic plate bender (APB) v1 is designed for simple straight plates with constant-pitch hole spacings and APB v2 is designed to accommodate more complex plates with in-plane curvature and variable-pitch hole spacings. In each system, the CMF fixture plate is indexed through the machine in a hole-to-hole fashion. Each hole is la-

beled 1 through K. At a given hole location k, the machine engages with the k^{th} and $k+1^{th}$ hole with two grippers that each have a cone that passes through the hole and then a platten that distributes the clamping force across the boss surrounding the hole, such that bending strains are localized to the webbing between hole bosses; this feature is critical because strain must be minimzed at the hole to ensure surgical screws will thread through the holes. Each plate is then sequentially bent, starting with a bend between holes 1 and 2 and ending with holes K-1 and K. APBs v1 and v2 are similar in design to other plate bending systems for POCM [9]. The contributions of this paper are:

- A formal kinematic description of the two POCM systems. As opposed to general six degree of freedom manipulators to achieve the bending tasks, the two systems are novel and designed to be minimal, purpose driven tools for a specific class of workpieces such that a compact machine could be integrated at the point of care (POC). Thus, the kinematics of the systems have not been described and require kinematic analysis to understand the classes of plates that can be formed, and the classes of bends that are achievable.
- Manipulability analysis to understand ill-posed configurations in the configuration space.
- Case studies that demonstrate simple path planning algorithms to avoid ill-posed configurations.

Section 2 describes a rigid body formalism to describe plate geometry and a bend a given hole *k*. Section 3 provides the methods of analysis for inverse kinematics and manipulability analysis, to assess which classes of plates and bends are achievable with each APB. Section 4 provides two case studies to show the implications of manipulability on APB v2 function, and a simple path planning algorithm to accommodate singularities in APB v2 mechanism configuration space. Section 5 provides a summary of major findings and future research directions.

2. Systems Descriptions

The rigid-body transformations used herein use the convention defined in [4] where the homogeneous transformation of frame $\{b\}$ in $\{a\}$, T_{ab} , is in the special Euclidean group SE(3)

$$T_{ab} = \left[\frac{R|p}{0|1}\right] \in SE(3) \tag{1}$$

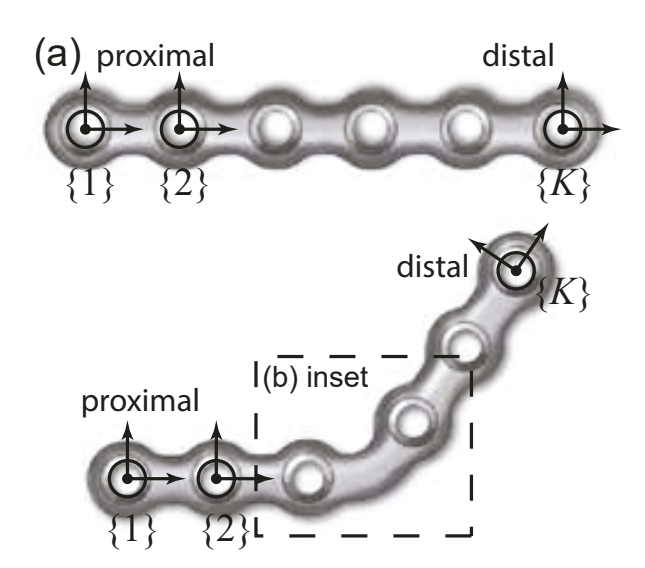
where the rotation matrix R is in the special orthogonal group SO(3) and the position vector $p \in \mathbb{R}^3$. Forward kinematics and the Jacobian will be defined in the space frame $\{s\}$ and using the methods of defining screw axes $S = [\omega, v]^T$ and the matrix exponential $T = e^{[S]\theta}$, where $\omega = [\omega_x, \omega_y, \omega_z]^T$ is the screw axis

angular velocity, $v = [v_x, v_y, v_z]^T$ is the screw axis linear velocity, and $\theta \in \mathbb{R}$ is the joint rotation. [S] denotes the structure

$$[S] = \begin{bmatrix} [\omega] \ v \\ 0 \ 0 \end{bmatrix}, \tag{2}$$

where $[\omega]$ is the skew-symmetric form of the vector ω . Trigonometric functions cos and sin will be given by the standard short-hand: $\cos\theta_1 = c_1$; $\cos(\theta_1 + \theta_2) = c_{12}$; $\sin\theta_1 = s_1$; $\sin(\theta_1 + \theta_2) = s_{12}$. The following will define the frames for the workpiece, define the kinematics of a plate bend, and then define the screw axes, forward kinematics, analytic Jacobian, and inverse kinematics for each testbed.

2.1. Kinematic description of the workpiece.



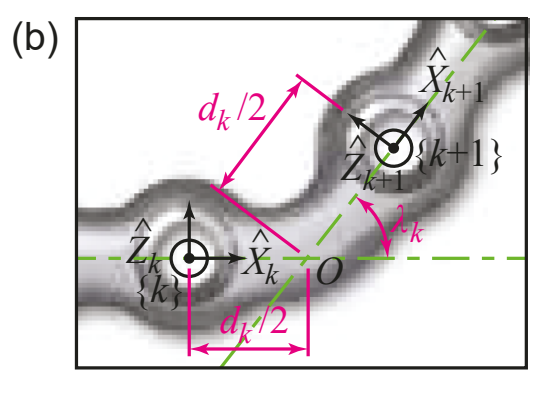


Figure 2. Fixation hardware workpiece description. (a) Representative geometries of a straight, constant-pitch fixation plate and a curved, variable-pitch fixation plate; (b) General representation of frames $\{k\}$ and $\{k+1\}$ for two adjacent holes in a fixation plate.

As described in Section 1, the workpiece is a standard craniofacial fixation plate, which, as received, is flat, such that all

features of interest are in the same plane (Fig. 2a). Each plate is composed of a series of holes arrayed along the length of the plate and these holes will be used as through holes for screws that fix the plate to the craniofacial structure. Each system is designed such that the gripper end effectors engage with two adjacent holes. Accordingly, we attach a sequence of frames to the geometric center of each hole, frames $\{1\} - \{K\}$. Prior to bending, the X-axis of the k^{th} frame, \hat{X}_k , is aligned parallel to the local tangent of the fixation plate (Fig. 2b). This creates a geometry where λ_k is the angle between the \hat{X}_k and \hat{X}_{k+1} axes and the Z-axes of each frame are aligned parallel to the \hat{Z}_0 of the Systems (Section 2.3. The pitch d_k is twice the distance between origin of $\{k\}$ and the intersection of \hat{X}_k and \hat{X}_{k+1} , point O. For adjacent holes that have \hat{X}_k parallel to \hat{X}_{k+1} – locally straight sections – the point O is half the distance between the frames. Given these frame definitions, the homogeneous transform between adjacent frames, and therefore fixation plate holes, is

$$T_{k,k+1}(\lambda_{k}, d_{k}) = \operatorname{Trans}\left(\hat{X}, \frac{d_{k}}{2}\right) \operatorname{Rot}\left(\hat{Z}, \lambda_{k}\right) \operatorname{Trans}\left(\hat{X}, \frac{d_{k}}{2}\right)$$

$$= \begin{bmatrix} c_{\lambda_{k}} - s_{\lambda_{k}} & 0 & \frac{d_{k}}{2} & (c_{\lambda_{k}} + 1) \\ s_{\lambda_{k}} & c_{\lambda_{k}} & 0 & \frac{d_{k}}{2} & s_{\lambda_{k}} \\ 0 & 0 & 1 & 0 \\ \hline 0 & 0 & 0 & 1 \end{bmatrix}.$$
(3)

where Trans and Rot are the standard translation and rotation operators for rigid body transforms. Accordingly, the homogenous transform for any two non-adjacent frames $\{k+m\}$ in frame $\{k\}$ is,

$$T_{k,k+m} = \prod_{i=0}^{n-1} T_{k+i,k+i+1},$$
(4)

where \prod indicates the right-multiply product.

2.2. Definition of the kinematics of a plate bend

As stated in Section 1, the fundamental purpose of both APBs is to incrementally bend a fixation plate workpiece. In the language of rigid body transforms, at a given set of frames, $\{k\}$ and $\{k+1\}$, the general task is to impart a three-axis bend, defined by angles α_k , β_k , γ_k , (yaw, pitch, roll, respectively) such that the $\{k+1\}$ frame is transformed to a bent frame $\{k+1\}'$ frame:

$$T_{k,k+1'} = T_{k,k+1} \Delta T(\alpha_k, \beta_k, \gamma_k), \tag{5}$$

where $\Delta T(\alpha_k, \beta_k, \gamma_k)$ is the homogenous transform of the imposed bend. The derivation of $\Delta T(\alpha_k, \beta_k, \gamma_k)$ assumes that bending is localized to the intersection of axes \hat{X}_k and \hat{X}_{k+1} of frames $\{k\}$ and $\{k+1\}$, respectively, and that bending is a pure rotation that does not stretch the plate, such that the distance between the origins between $\{k\}$ and $\{k+1\}$ and intersection O are invariant to bending. Given these assumptions,

$$T_{k,k+1'} = \operatorname{Trans}\left(\hat{X}, \frac{d_k}{2}\right) \operatorname{Rot}\left(\hat{Z}, \lambda_k\right) \operatorname{Rot}\left(\hat{Z}, \alpha_k\right) \operatorname{Rot}\left(\hat{Y}, \beta_k\right) \operatorname{Rot}\left(\hat{X}, \gamma_k\right) \operatorname{Trans}\left(\hat{X}, \frac{d_k}{2}\right)$$

$$= \begin{bmatrix} c_{\lambda_k \alpha_k} c_{\beta_k} & c_{\lambda_k \alpha_k} s_{\beta_k} s_{\gamma_k} - s_{\lambda_k \alpha_k} c_{\gamma_k} & c_{\lambda_k \alpha_k} s_{\beta_k} c_{\gamma_k} + s_{\lambda_k \alpha_k} s_{\gamma_k} & \frac{d_k}{2} \left(c_{\lambda_k \alpha_k} c_{\beta_k} + 1\right) \\ s_{\lambda_k \alpha_k} c_{\beta_k} & s_{\lambda_k \alpha_k} s_{\beta_k} s_{\gamma_k} + c_{\lambda_k \alpha_k} c_{\gamma_k} & s_{\lambda_k \alpha_k} s_{\gamma_k} & \frac{d_k}{2} s_{\lambda_k \alpha_k} c_{\beta_k} \\ -s_{\beta_k} & c_{\beta_k} s_{\gamma_k} & c_{\beta_k} c_{\gamma_k} & -\frac{d_k}{2} s_{\beta_k} \\ \hline 0 & 0 & 1 \end{bmatrix}.$$

$$(6)$$

and therefore

$$\Delta T_{k} = \operatorname{Trans}^{-1}\left(\hat{X}, \frac{d_{k}}{2}\right) \operatorname{Rot}\left(\hat{Z}, \lambda_{k}\right) \operatorname{Rot}\left(\hat{Z}, \alpha_{k}\right) \operatorname{Rot}\left(\hat{Y}, \beta_{k}\right) \operatorname{Rot}\left(\hat{X}, \gamma_{k}\right) \operatorname{Trans}\left(\hat{X}, \frac{d_{k}}{2}\right)$$

$$= \begin{bmatrix} c_{\alpha_{k}} c_{\beta_{k}} c_{\alpha_{k}} s_{\beta_{k}} s_{\gamma_{k}} - s_{\alpha_{k}} c_{\gamma_{k}} c_{\alpha_{k}} s_{\beta_{k}} c_{\gamma_{k}} + s_{\alpha_{k}} s_{\gamma_{k}} & \frac{d_{k}}{2} \left(c_{\alpha_{k}} c_{\beta_{k}} - 1\right) \\ s_{\alpha_{k}} c_{\beta_{k}} s_{\alpha_{k}} s_{\beta_{k}} s_{\gamma_{k}} + c_{\alpha_{k}} c_{\gamma_{k}} s_{\alpha_{2}} s_{\beta_{k}} c_{\gamma_{k}} - c_{\alpha_{k}} s_{\gamma_{k}} & \frac{d_{k}}{2} s_{\alpha_{k}} c_{\beta_{k}} \\ -s_{\beta_{k}} c_{\beta_{k}} s_{\gamma_{k}} & c_{\beta_{k}} c_{\gamma_{k}} & -\frac{d_{k}}{2} s_{\beta_{k}} \\ \hline 0 & 0 & 1 \end{bmatrix}.$$

$$(7)$$

Analogous to Eq. (4), the homogenous transform for any two non-adjacent frames $\{k + m'\}$ in frame $\{k\}$ after bending is,

$$T_{k,k+m'} = \prod_{i=0}^{n-1} T_{k+i,k+i+1} \Delta T(\alpha_{k+i}, \beta_{k+i}, \gamma_{k+i}).$$
 (8)

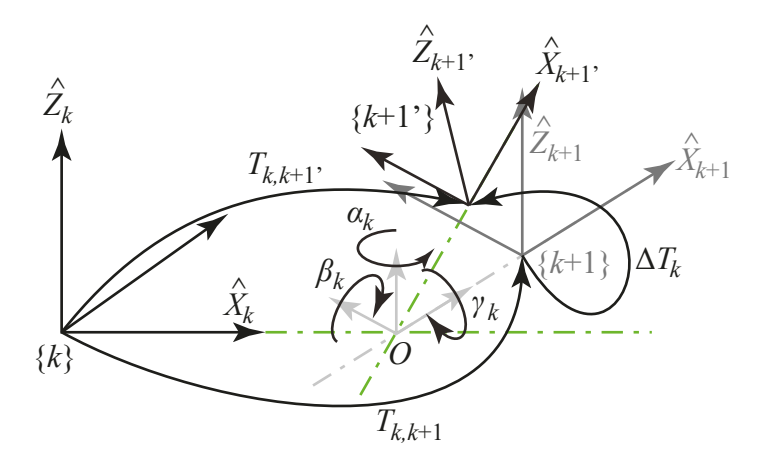


Figure 3. Kinematic description of a bend.

2.3. Kinematic description of the systems

APBs v1 and v2 are multi-joint, thus multi-degree-of-freedom robotic systems. APB v1 is a Revolute-Prismatic-Revolute (RPR) mechanism with n=3 joints: two R joints and one P joint. APB v2 is a RPRPR mechanism with n=5 joints: three R joints and two P joints.

Both APBs v1 and v2 operate in the following sequence. At each incremental bend:

- 1. The gripping end-effector labeled by frame {0} engages with the {k} frame of the workpiece.
- 2. The gripping end-effector labelled by frame $\{n\}$ engages with the $\{k+1\}$ frame of the workpiece.
- 3. A path is executed to impose a bend in the plate, by actuating joints $\theta = [\theta_1 \theta_n]^T$, to impose an additional transformation $T_{k,k+m'} = T_{k,k+1} \Delta T(\alpha_k, \beta_k, \gamma_k)$, where $T_{k,k+1}$ is the as-received rigid-body transform in the plate, and $\Delta T(\alpha_k, \beta_k, \gamma_k)$ is the imposed plate deformation, as described in Section 2.2.
- 4. The gripping end-effector labelled by frame $\{n\}$ disengages with the $\{k+1\}$ frame of the workpiece to release the workpiece on the distal end.
- 5. The gripping end-effector labelled by frame $\{n\}$ engages with the $\{k+2\}$ frame of the workpiece to index along the plate.

- 6. The gripping end-effector labelled by frame {0} disengages with the {*k*} frame of the workpiece to release workpiece on the proximal end.
- 7. The incremental cycle starts anew: k = k + 1.

The kinematics analysis presented here describes all bend motions relative to the {0}-frame labeled in Fig. 4, imposing the {0}-frame as a virtual base. Note that the physical base indicated in the figure is not a convenient base frame for describing bends, and is assumed to be moving with reference to the {0}-frame.

Given the screw axes labels and angle definitions in Fig. 4, the space screw axes in Tables 1 and 2 provide the kinematic parameters of each system.

Table 1. Space frame screw axes and joint position limits for APB v1.

S_i	ω_i	v_i	$\underline{\theta}$	$ar{ heta}$
S_1	{0, 1, 0}	$\{0,0,d\}$	-15 [deg]	30 [deg]
\mathcal{S}_2 \mathcal{S}_3	$\{0,0,0\}$ $\{1,0,0\}$	$\{1,0,0\}$ $\{0,0,0\}$	0 [mm] -30 [deg]	10 [mm] 30 [deg]

Table 2. Space frame screw axes and joint position limits for APB v2.

S_i	ω_i	v_i	$\underline{\theta}$	$ar{ heta}$
$\overline{S_1}$	{1, 0, 0}	{0, 0, 0}	-180 [deg]	180 [deg]
\mathcal{S}_2	$\{0, 0, 0\}$	$\{1, 0, 0\}$	0 [mm]	20 [mm]
\mathcal{S}_3	$\{0, 0, 1\}$	$\{0, -d, 0\}$	-22.5 [deg]	22.5 [deg]
\mathcal{S}_4	$\{0, 0, 0\}$	{1, 0, 0}	0 [mm]	20 [mm]
\mathcal{S}_5	$\{1, 0, 0\}$	$\{0, 0, 0\}$	-180 [deg]	180 [deg]

The null configurations for both system are given by:

$$M = \begin{bmatrix} I & 2d \\ 0 & 0 \\ \hline 0 & 1 \end{bmatrix}. \tag{9}$$

2.4. Forward kinematics

The forward kinematics of a mechanism is given by

$$T_{0n}(\theta) = e^{[S1]\theta_1} \dots e^{[Sn]\theta_n} M. \tag{10}$$

Accordingly, the forward kinematics for APB v1 is given by

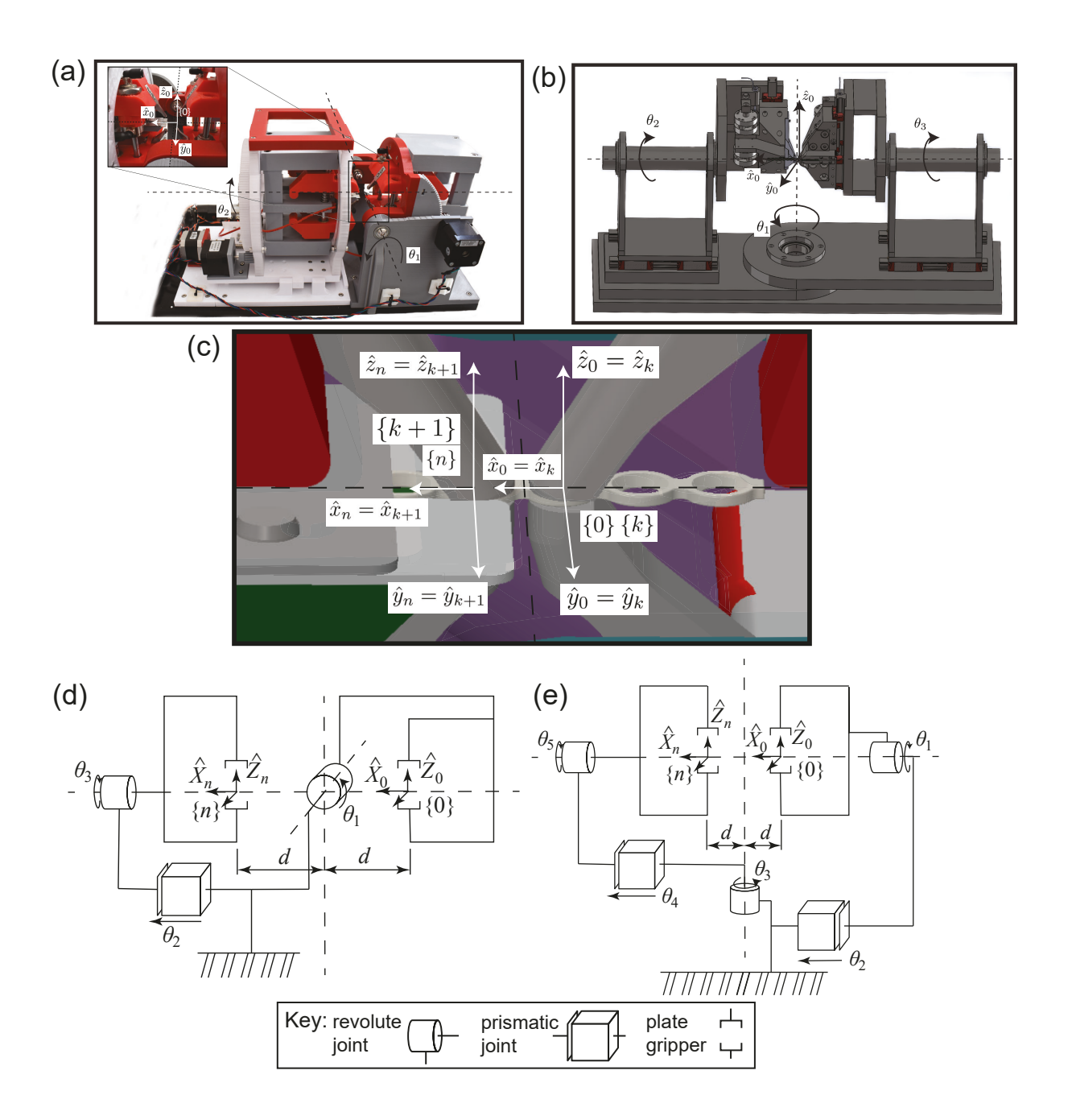


Figure 4. Kinematic diagram of APBs v1 and v2. (a) APB v1 physical hardware; (b) CAD model of APB v2; (c) Detail of the engagement between the gripper end effectors, frame $\{0\}$ and $\{n\}$, and two adjacent hole frames on the plate, frames $\{k\}$ and $\{k+1\}$; (d) Kinematics schematic for APB v1; (e) Kinematics schematic for APB v2.

Note, that only θ_1 and θ_3 are present in the rotation of matrix of $T_{03}(\theta)$ and the Y component of the position vector is zero,

$$T_{03}(\theta) = \begin{bmatrix} c_1 & s_1 s_3 & s_1 c_3 \\ 0 & c_3 & -s_3 \\ -s_1 & c_1 s_3 & c_1 c_3 \\ \hline 0 & 0 & 0 \end{bmatrix} \begin{pmatrix} c_1 (\theta_2 + d) + d \\ 0 & c_3 - s_1 (\theta_2 + d) \\ \hline 0 & 0 & 0 \end{bmatrix}.$$
(11)

which will have implications on the types of plates APB v1 can bend and the achievable bends.

The forward kinematics for APB v2 is given by

$$T_{05}(\theta) =$$

$$\begin{bmatrix} c_3 & -s_3c_5 & s_3s_5 & c_3(\theta_4+d)+\theta_2+d \\ c_1s_3 & c_1c_3c_5 - s_1s_5 - c_1c_3s_5 - s_1c_5 & c_1s_3(\theta_4+d) \\ s_1s_3 & s_1c_3c_5 + c_1s_5 - s_1c_3s_5 + c_1c_5 & s_1s_3(\theta_4+d) \\ \hline 0 & 0 & 1 \end{bmatrix}.$$
(12)

Note the additionally complexity and lack of zero entries in both the rotation matrix and position vector of (12) in comparison to (11), which expands the set of plates that APB v2 can bend, and the achievable bend complexity.

3. Analysis Methodology and Results

APBs v1 and v2 are analyzed using the inverse kinematics analysis to understand the reachable workspace, both in terms of the classes of standard plates that a system can engage with and the classes of bends each system can make, and manipulability analysis to understand configuration space singularities and condition number analysis to understand ill-posed configurations.

3.1. Inverse Kinematics

The inverse kinematics for each system is the solution for the joint angles $\theta_1 - \theta_n$ for each system, to achieve the required end-effector homogeneous solution $T_{k,k+1}$, Eqn. (3), to engage with the plate before a bend, and $T_{k,k+1}$, Eqn. (6), to bend the plate to the desired bend angles.

3.1.1. APB v1 for plate engagement

 $\theta_1 - \theta_3$ are solved by equating Eqn. (3) to Eqn. (11). As can be seen by comparing matrix entries, APB v1 can only engage with straight fixation plate workpieces and the hole pitch for each hole must be $d_k = d$. For workpieces in which these constraints are satisfied, the inverse kinematic solution is,

$$\theta_1 = 0$$

$$\theta_2 = 0$$

$$\theta_3 = 0$$
(13)

3.1.2. APB v1 to complete a bend

 $\theta_1 - \theta_3$ are solved by equating Eqn. (6) to Eqn. (11). As can be seen by comparing matrix entries, APB v1 can cannot perform non-zero α bends – yaw bends. For bend requirements constrained such that $\alpha = 0$,

$$\theta_1 = \beta$$

$$\theta_2 = 0$$

$$\theta_3 = \gamma$$
(14)

3.2. APB v2 for plate engagement

 $\theta_1 - \theta_5$ are solved by equating Eqn. (3) to Eqn. (12). In contrast to APB v1, there does exist an inverse kinematics solution for $\lambda_k \neq 0$ and $\frac{d_k}{2} \neq d$, and thus APB v2 can engage with curved and variable pitch fixation plate workpieces.

$$\theta_{1} = 0$$

$$\theta_{2} = \frac{d_{k}}{2} - d$$

$$\theta_{3} = \lambda_{k}$$

$$\theta_{4} = \frac{d_{k}}{2} - d$$

$$\theta_{5} = 0$$
(15)

3.2.1. APB v2 to complete a bend

 $\theta_1 - \theta_5$ are solved by equating Eqn. (6) to Eqn. (12). Note that the solution set below is in the required order of solution, not in numerical order.

$$\theta_{3} = \operatorname{atan2}\left(\pm\sqrt{1 - (c_{\beta_{k}}c_{\lambda_{k}\alpha_{k}})^{2}}, c_{\beta_{k}}c_{\lambda_{k}\alpha_{k}}\right)$$

$$\theta_{1} = \operatorname{atan2}\left(-\frac{s_{\beta_{k}}}{s_{3}}, \frac{c_{\beta_{k}}s_{\lambda_{k}\alpha_{k}}}{s_{3}}\right)$$

$$for \theta_{3} \neq 0, \pm 180^{\circ}, \pm 360^{\circ}, \dots$$

$$\theta_{2} = \frac{d_{k}}{2} - d$$

$$\theta_{4} = \frac{d_{k}}{2} - d$$

$$\theta_{5} = \operatorname{atan2}\left(\frac{1}{s_{3}}\left(s_{\beta_{k}}c_{\gamma_{k}}c_{\lambda_{k}\alpha_{k}} + s_{\gamma_{k}}s_{\lambda_{k}\alpha_{k}}\right), -\frac{1}{s_{3}}\left(s_{\beta_{k}}s_{\gamma_{k}}c_{\lambda_{k}\alpha_{k}} - c_{\gamma_{k}}s_{\lambda_{k}\alpha_{k}}\right)\right)$$

$$for \theta_{3} \neq 0, \pm 180^{\circ}, \pm 360^{\circ}, \dots$$

An inverse kinematics solution exists, provided that $\beta_k \neq 0$ or $\alpha_k \neq -\lambda_k$; this means that given that there is a pitch bend $\beta_k \neq 0$ or that the yaw bend α_k is not specified to straighten out the asreceived bend in the plate $(\lambda_k \neq 0)$ or, the more likely scenario, there is no yaw bend on a straight plate $(\alpha_k = 0 \text{ and } \lambda_k = 0)$, APB v2 can apply the bend. Additionally, note that there are two solutions for θ_3 , which is typical in mechanisms with revolute joints. Additionally, note the invariance of θ_2 and θ_4 to the bend angles α_k , β_k , and γ_k , prescribing that the prismatic joints θ_2 and θ_4 will be fixed after plate engagement and during a bend.

3.3. Singularity and Manipulability Analysis

The space-frame Jacobian is given by,

$$J_{s} = \left[(S_{1}) \operatorname{Ad}_{e}[s_{1}]^{\theta_{1}} (S_{2}) \cdots \operatorname{Ad}_{e}[s_{1}]^{\theta_{1}} ... e^{[S_{n-1}]^{\theta_{n-1}}} (S_{n}) \right], \quad (17)$$

where the adjoint operator Ad_T is

$$Ad_T = \begin{bmatrix} R & 0 \\ [p] R R \end{bmatrix}. \tag{18}$$

A robotic mechanism is at a singularity if Rank $(J_s) < n$.

The application of Eqn. (17) to the kinematics of APB v2 yields the space Jacobian

$$J_{s} = \begin{bmatrix} 0 & 0 & c_{1} \\ 0 & 0 & 0 \\ \frac{1}{0} & c_{1} & 0 \\ 0 & 0 & ds_{1} \\ d - s_{1} & 0 \end{bmatrix}.$$
 (19)

 J_s is not a function of θ_2 nor θ_3 , and thus no values of θ_2 or θ_3 will yield a singular configuration. Rank analysis of J_s also indicates that J_s is not rank deficient for any value of θ_1 .

The application of Eqn. (17) to the kinematics of APB v2 yields the space Jacobian

$$J_{s} = \begin{bmatrix} 1 & 0 & 0 & 0 & c_{3} \\ 0 & 0 & -s_{1} & 0 & c_{1}s_{3} \\ 0 & 0 & c_{1} & 0 & s_{1}s_{3} \\ \hline 0 & 1 & 0 & c_{3} & 0 \\ 0 & 0 - c_{1}(\theta_{2} + d) & c_{1}s_{3} - s_{1}s_{3}(\theta_{2} + d) \\ 0 & 0 - s_{1}(\theta_{2} + d) & s_{1}s_{3} & c_{1}s_{3}(\theta_{2} + d) \end{bmatrix}.$$
(20)

 J_s is not a function of θ_4 or θ_5 , and thus no values of θ_4 or θ_5 will yield a singular configuration. Rank analysis J_s also indicates that J_s is rank deficient when $\theta_3 = 0, \pm 180^{\circ}, \ldots$; however, given the joint limits in Tb. 2, the only relevant singularity is $\theta_3 = 0^{\circ}$.

Additionally, the Jacobian can be partitioned into an angular velocity and a linear velocity component $J_s = [J_{\omega_s}, J_{\nu_s}]^T$ to investigate a metric of closeness to a singularity, termed the condition number for the angular velocity or linear velocity components. Given the manipulability of a bend is tied to the angular velocity component of the Jacobian, the condition number used here is

$$\mu_{\omega} = \frac{\max eig\left(J_{\omega_{s}}J_{\omega_{s}}^{\mathrm{T}}\right)}{\min eig\left(J_{\omega_{s}}J_{\omega_{s}}^{\mathrm{T}}\right)},\tag{21}$$

where eig (\cdot) is eigenvalue operator and $\mu_{(\cdot)} \ge 1$, and a $\mu_{(\cdot)}$ that is close to 1 indicates a well-posed J_s that is not close to a singularity and a large $\mu_{(\cdot)}$ indicates an ill-posed configuration. Not suprisingly, $\mu_{\omega} = \infty$ for every configuration for APB v1, indicating a lack of ability to move in the yaw direction. For APB v2, J_{ω_s} is a function of θ_1 and θ_3 , as seen in Eqn. 20; the contour plot of condition number μ_{ω} over the range of θ_1 and θ_3 is shown in Fig. 5. μ_{ω} has a strong peak at the known singularity of $\theta_3 = 0$. μ_{ω} is not a function of θ_1 . Accordingly, path planning algorithms for a bend should be designed to avoid ill-posed configurations near $\theta_3 = 0$.

4. Case Studies

Two case studies are devised that test the ability of a simple path planning algorithm to navigate the singularity in the configuration space for APB v2. Two sets of plate designs and final bend angles are chosen such that the starting configuration is near the singularity of $\theta_3=0$, Tb. 3, to stress the ability of the algorithm to find a solution path while in the vicinity of the singularity. A simple lowest cost path search algorithm [3] is used with a cost function, $L(\theta)$, that is composed of the summation of the condition number as a cost penalty and the distance to a final bend configuration as a goal potential well to attact solution,

$$L(\theta) = \mu_{\omega}(\theta) + \rho \min\left(||\theta_{end,1} - \theta||, ||\theta_{end,2} - \theta||\right). \tag{22}$$

 $\theta_{1,end}$ and $\theta_{2,end}$ are the two solutions to Eqn. (16), and thus the two options for the configuration that completes the bend: $\theta_{1,end}$ is the + solution and $\theta_{2,end}$ is the - solution $\rho \in \mathbb{R}$ weights the relative penalty of each term, and $\rho = \frac{1}{10}$ [1/deg] is heuristically chosen here. A contour plot of the cost function for each case is shown in Fig. 6. The lowest cost path is then filtered with a

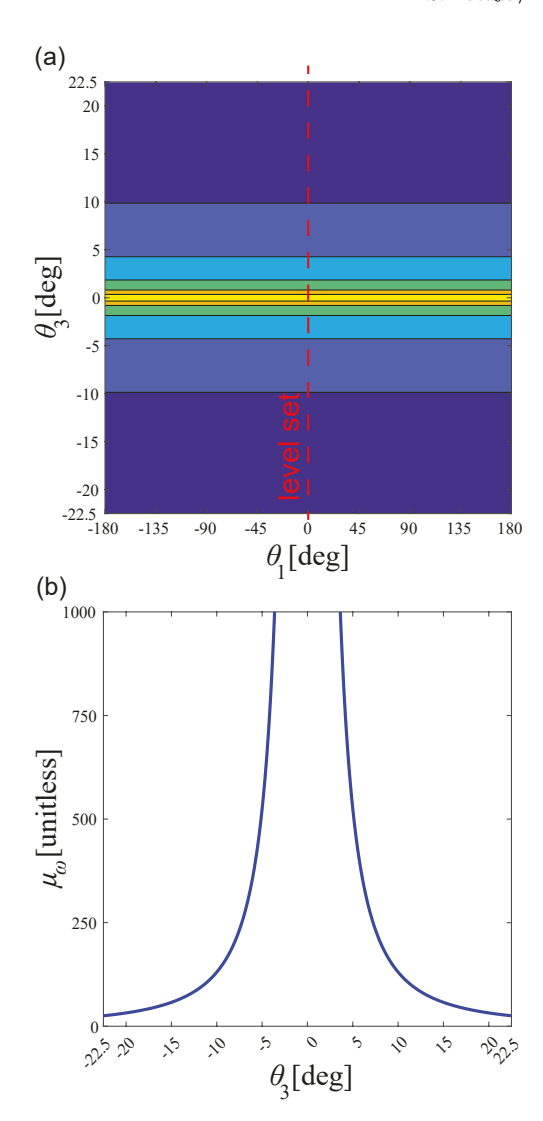
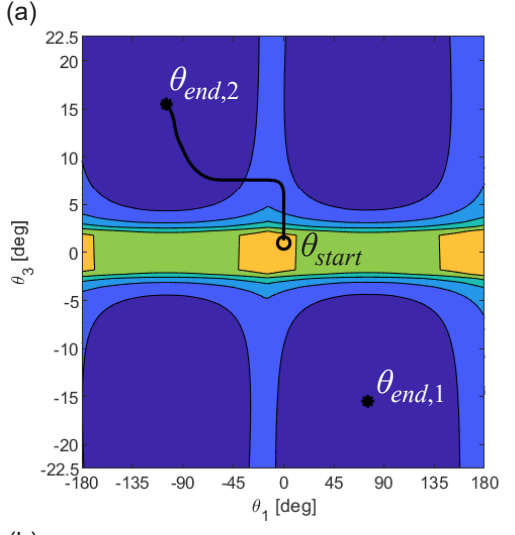


Figure 5. Manipulability analysis of APB v2. (a) Contour plot of the \log_{10} of condition number μ_{ω} over the configuration space of θ_1 and θ_3 . (b) Level set of μ_{ω} to demonstrate the dependence of the condition number of θ_3 . $\mu_{\omega}=\infty$ at $\theta_3=0$.

zero-phase moving average filter to smooth the path [4]. The paths for the two cases demonstrate that the path planning algorithm both finds the solution, $\theta_{1,end}$ vs. $\theta_{2,end}$, that completes the bend without crossing the singularity and also steeply follows the gradient in $L(\theta)$ to incur the least amount of loss in the path. In terms of the joints of APB v2, if θ_3 is near the singularity at $\theta_3 = 0$, the algorithm will choose the correct direction to rotate θ_3 , and rotate θ_3 first to get away from the singularity, and then, once sufficiently far from the singularity, the other joints will rotate to converge to the solution.

Table 3. Plate geometry and bend angles for two different Case scenarios.

Case No.	λ_k	α_k	$oldsymbol{eta}_k$	γ_k
1	1°	-5°	15°	10°
2	-1°	-7°	15°	20°



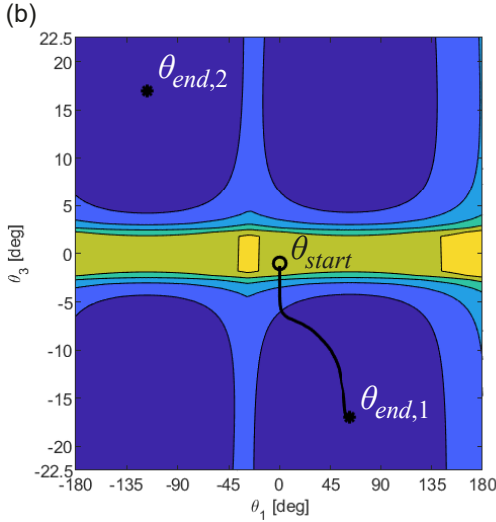


Figure 6. Motion paths for Cases 1 (a) and 2 (b), superimposed on a contour plot of cost function $L(\theta)$. The starting configuration θ_{start} and the two solutions to Eqn. (16) for the ending configuration, $\theta_{end,1}$ and $\theta_{end,2}$, are shown. The path planning algorithm finds a path the incurs the lowest cost to get to one of the two solutions.

5. Summary and Conclusions

A complete reachable workspace analysis via inverse kinematics and manipulability analysis demonstrate the key kinematic features of each system. The critical findings are summarized in Tb. 4. APB v1 is a simple, minimal mechanism for applications in which straight, constant pitch CMF fixation plates are to be used and the plates are only to be bent in pitch and roll ($\beta \neq 0$, $\gamma \neq 0$, and $\alpha = 0$) directions. APB v2 has two more active joints, which expands the classes of plates and bends that can be engaged with and achieved, respectively; APB v2 can engage with curved, variable pitch CMF fixation plates and can achieve bends in all three directions ($\alpha \neq 0$, $\beta \neq 0$, and $\gamma \neq 0$). APB v2 does have a singularity in the configuration space, as is typical with gimbal mechanisms in which three revolute joints intersect at a single point (point O on the fixation plate) [4];

however, this singularity can be managed with simple path planning algorithms, as demonstrated in the case studies in Section 4.

Table 4. Summary of Results. An x indicates that a system is capable of specified engagement or bend.

Property	APB v1	APB v2
Engagement		
Straight Plates $(\lambda_k = 0)$	X	X
Curved Plates $(\lambda_k \neq 0)$		X
Constant Pitch $(\frac{d_k}{2} = d)$	X	X
Curved Plates $(\frac{d_k}{2} \neq d)$		X
Bend		
Yaw Bend $(\alpha_k \neq 0)$		X
Pitch Bend ($\beta_k \neq 0$)	X	X
Roll Bend $(\gamma_k \neq 0)$	X	x

This fundamental study of mechanism kinematics for the APBs is just the first of a few on the study of the mechanism of increment forming in the POCM workflow. It is wellknown that incremental forming of Ti-6Al-4V plates will exhibit springback, where the actual bend after gripper disengagment will not match the imposed bend from the actuated joints [6, 7]. Future research will investigate closed-loop control systems for the APB in which the actual bend angles will be measured with on board sensors and multiple incremental bends will be applied to ensure that the actual bend matches the desired bend to a clinically relevant threshold [1]. As is clinically known from a heurisitic point of view, excessive incrememental forming will cause work hardening, which embrittles the CMF plates and increases the probability of cyclic fatigue failure. Work hardening estimator need to be integrated to place constraints on the feedback control system to improve the fatigue life of CMF plates, and hence improve patient outcomes. Lastly, there are classes of plates that are pre-bent in the pitch and roll axes, and thus do not satisfisfy the plate definitions from Section 2.1; engagement and bending manipulability must be studied for this more expansive set of clinically relevant plates.

Acknowledgements

The authors would like to acknowledge support from the NSF Engineering Research Center for Hybrid Autonomous Manufacturing Moving from Evolution to Revolution (ERC-HAMMER) under Award Number EEC-2133630.

References

- [1] Allwood, J.M., Duncan, S.R., Cao, J., Groche, P., Hirt, G., Kinsey, B., Kuboki, T., Liewald, M., Sterzing, A., Tekkaya, A.E., 2016. Closed-loop control of product properties in metal forming. CIRP Annals 65, 573–596. URL: https://www.sciencedirect.com/science/article/pii/S0007850616301949, doi:https://doi.org/10.1016/j.cirp.2016.06.002.
- [2] Claes, L., Augat, P., Suger, G., Wilke, H.J., 1997. Influence of size and stability of the osteotomy gap on the success of fracture healing. Journal

- of Orthopaedic Research 15,577-584. URL: https://onlinelibrary.wiley.com/doi/abs/10.1002/jor.1100150414, doi:https://doi.org/10.1002/jor.1100150414.
- [3] Luong, B., 2021. Shortest path in a 2d matrix. URL: https://www.mathworks.com/matlabcentral/answers/722518-shortest-path-in-a-2d-matrix.
- [4] Lynch, K.M., Park, F.C., 2019. Modern robotics: mechanics, planning, and control. Reprinted with additions and corrections ed., Cambridge University Press, Cambridge New York, NY Port Melbourne.
- [5] Moghaddam, N.S., Skoracki, R., Miller, M., Elahinia, M., Dean, D., 2016. Three Dimensional Printing of Stiffness-tuned, Nitinol Skeletal Fixation Hardware with an Example of Mandibular Segmental Defect Repair. Procedia CIRP 49, 45-50. URL: https://www. sciencedirect.com/science/article/pii/S2212827115007866, doi:https://doi.org/10.1016/j.procir.2015.07.027.
- [6] Ren, H., Xie, J., Liao, S., Leem, D., Ehmann, K., Cao, J., 2019. Insitu springback compensation in incremental sheet forming. CIRP Annals 68, 317–320. URL: https://linkinghub.elsevier.com/retrieve/pii/S000785061930068X, doi:10.1016/j.cirp.2019.04.042.
- [7] Tekkaya, A.E., Allwood, J.M., Bariani, P.F., Bruschi, S., Cao, J., Gramlich, S., Groche, P., Hirt, G., Ishikawa, T., Löbbe, C., Lueg-Althoff, J., Merklein, M., Misiolek, W.Z., Pietrzyk, M., Shivpuri, R., Yanagimoto, J., 2015. Metal forming beyond shaping: Predicting and setting product properties. CIRP Annals 64, 629–653. URL: https://www.sciencedirect.com/science/article/pii/S0007850615001407, doi:https://doi.org/10.1016/j.cirp.2015.05.001.
- [8] Vazquez-Armendariz, J., Olivas-Alanis, L.H., Mahan, T., Rodriguez, C.A., Groeber, M., Niezgoda, S., Morris, J.M., Emam, H., Skoracki, R., Cao, J., Ripley, B., Iaquinto, J., Daehn, G., Dean, D., 2023. Workflow for Robotic Point-of-Care Manufacturing of Personalized Maxillofacial Graft Fixation Hardware. Integrating Materials and Manufacturing Innovation 12, 92–104. URL: https://doi.org/10.1007/s40192-023-00298-3, doi:10.1007/s40192-023-00298-3.
- Zhang, J., Shi, B., Feng, G., Zuo, G., Liang, Y., 2022. Design, development and control of a forming robot for an internally fixed titanium alloy strip. Machines 10. URL: https://www.mdpi.com/2075-1702/10/2/68, doi:10.3390/machines10020068.